

Can ring current stabilize magnetotail during steady magnetospheric convection?

S. Dubyagin,¹ N. Ganushkina,^{1,2} M. Liemohn,² M. Kubyshkina,³

Corresponding author: S. Dubyagin, Earth Observation department, Finnish Meteorological Institute, Erik Palmenin aukio 1, Helsinki, FI-00101, Finland. (stepan.dubyagin@fmi.fi)

¹Earth Observation department, Finnish Meteorological Institute, Helsinki, Finland.

²University of Michigan, Ann Arbor, Michigan, USA

³St. Petersburg State University, St. Petersburg, Russia

Abstract. The present study investigates the role of the ring current in stabilizing the magnetotail during Steady Magnetospheric Convection (SMC) events. We develop a method for estimation of the symmetric ring current intensity from the single spacecraft magnetic field observations. The method is applied to a large number of SMC events identified using three different automatic procedures adopted from the literature. It is found that the symmetric ring current can be weak or strong depending on a particular event. We find a significant fraction of events that have a rather weak symmetric ring current in spite of the strong solar wind driving during the event. These findings imply that the symmetric ring current plays no role in the magnetotail stabilization.

1. Introduction

The intervals known as Steady Magnetospheric Convection (SMC) have been attracting scientists' attention for a few decades [see a review by *Sergeev et al.*, 1996]. The puzzle of SMC is why a substorm does not occur during this period in spite of strong solar wind driving. At the same time, *Kissinger et al.* [2012] claimed that 99% of SMCs are preceded by substorms.

It is known that substorms can inject particles into the ring current region. It was also found that the critical value of the magnetic flux in the lobe, above which the substorm onset occurs, depends on the SYM-H index [*Nakai and Kamide*, 2003; *Milan et al.*, 2009]. The stronger SYM-H, the more stable the magnetotail is. To explain this finding, *Milan et al.* [2009] speculated that the magnetic field of enhanced ring current penetrates into the tail current region and stabilizes the current sheet. *Juusola et al.* [2013] adapted this scenario for an explanation of the magnetospheric stability during SMC periods. The authors analyzed a large number of SMC events and found that SYM-H is often moderately negative (some tens of nanotesla). According to *Juusola et al.* [2013], the estimated ring current, which creates such depression at the ground, would produce a prominent positive B_Z in the magnetotail region. It is known that the small normal component of the magnetic field in the current sheet is a necessary condition for tearing instability development [e.g. *Lembege and Pellat*, 1982; *Brittnacher et al.*, 1994; *Schindler*, 2007]. Thus, if the SYM-H index variation is produced by the symmetric ring current, the enhanced ring current might be a cause of why a substorm does not happen during an SMC. However, there are serious objections to this simple scenario. First (and the most

important), the proposed mechanism assumes a vacuum-like penetration of the magnetic field of the ring current in the central plasma sheet region, and neglects the existence of hot plasma in that region. The frozen-in condition is valid throughout the magnetotail most of the time. Therefore, any change of the magnetic field must be accompanied by plasma motion. At the same time, the convection in the highly dynamical plasma sheet region is mostly controlled by external solar wind driving, not by the inner-magnetosphere current reconfiguration.

Secondly, the usage of the SYM-H index as a measure of the symmetric ring current intensity is questionable [Alexeev *et al.*, 1996; Turner *et al.*, 2000; Liemohn *et al.*, 2001a, b; Maltsev, 2004; Ganushkina *et al.*, 2004; Kalegaev *et al.*, 2005; Ganushkina *et al.*, 2010]. SYM-H is definitely a good indicator of the ring current intensity during the storm recovery phase but this is not necessarily true during SMCs. However, we cannot fully rule out the possibility that the ring current somehow affects the threshold for magnetotail reconnection through the more complex chain of interactions.

Pulkkinen et al. [2013] analyzed the magnetic field in the inner magnetosphere for a large number of SMC events and compared these characteristics with a reference data set (representing average conditions). The authors found that the dayside magnetosphere compression is weaker in comparison to the reference data set. This finding was interpreted as a manifestation of the strong ring current.

The ring current intensity could be potentially obtained from the statistical empirical models. However, the family of Tsyganenko empirical models are generally fitted to all available data [Tsyganenko, 2013], hence representing a mixture of various dynamic states of the magnetosphere. In addition, to check the role of the ring current in stabilizing the

magnetotail, one needs to know the statistical distribution of the ring current strength during the SMC events rather than its average characteristics.

In this paper, we check if the magnetosphere, having relatively weak ring current, can resist strong solar wind driving during SMC events. The intensity of symmetric ring current is estimated for a large number of SMC events. The word “symmetric” means that this current flows around the earth, in contrast to the partial ring current, and we do not mean any symmetry in a strict sense (see recent review by *Ganushkina et al.* [2015] for more details on definitions of the magnetospheric current systems). Then we check if there is a dependence of the ring current intensity on a solar wind driving strength. If the hypothesis is correct, one would expect that the stronger the driver, the stronger the ring current needed to support the magnetotail stability. Actually, a part of the answer is already known as the strong ring current definitely exists during storm-time SMC events. However, in those cases, strong ring current and stability of the magnetotail could be independent of each other. In other words, even if the ring current is statistically stronger during the SMC events it does not mean that it plays any role in tail current sheet stabilization.

In Section 2 we discuss the criteria for the SMC events selection. The method of the ring current intensity estimation is presented in Section 3. Section 4 contains information about the spacecraft data. Validation of the method is presented in Section 5. The results of the study are presented in Section 6 and discussed in Section 7.

2. SMC interval selection

Different authors use different definitions for SMC events and different approaches for selection of the SMC intervals. While some studies use auroral electrojet indices together

with information about Interplanetary Magnetic Field (IMF) orientation and global auroral dynamics [e.g., *Sergeev et al.*, 1996; *Yahnin et al.*, 1994; *DeJong and Clauer*, 2005], others use solely auroral electrojet indices for selection of the SMC events [e.g., *O'Brien et al.*, 2002; *Kissinger et al.*, 2011; *Juusola et al.*, 2013; *DeJong*, 2014]. Unfortunately, it is always a trade off between selection quality and the number of events since the data from the solar wind and global auroral imagers are not always available.

For our study, we adapted three different criteria for selection of SMC events [*Kissinger et al.*, 2011; *Juusola et al.*, 2013; *DeJong*, 2014]. All these criteria use auroral electrojet indices (no information about IMF is used for selection, we discuss the limitation of such approach in the Discussion section). The *Kissinger et al.* [2011] and *DeJong* [2014] criteria also require visual inspection. According to *DeJong* [2014], visual inspection removes 15% of events from the automatically generated list. We did not perform any visual inspection, instead using only the automatic part of these criteria.

We applied the aforementioned selection techniques to 18 years (1996–2013) of auroral indices data (AE, AL, AU) and obtained three lists of events. Hereafter we will refer to the lists which were based on 1) *Kissinger et al.* [2011], 2) *Juusola et al.* [2013], and 3) *DeJong* [2014] criteria using the first authors names Kissinger, Juusola, and DeJong lists, respectively. However, we emphasize that these lists can be different from those used in the original studies (since we use only the automatic part of the original selection procedures). Table 1 summarizes the total duration and percentage of the time when the magnetosphere was in SMC conditions according to the different selection criteria. It can be seen that the DeJong procedure selects almost two times more events than other criteria. The DeJong procedure defines 7% of time as SMC intervals. The histogram

in Figure 1a shows the SMC event durations. The minimal length of SMC interval was limited by 1.5h for Kissinger and Juusola selection, and by 3h for DeJong selection. It can be seen that the DeJong criteria generally select longer SMC intervals.

Since IMF B_Z was not used for the selections, we check what fraction of a total event duration B_Z is negative. For each event, we computed the percentage of time when IMF B_Z was negative. Figure 1b shows the histogram of this percentage. It can be seen that for Kissinger and Juusola lists IMF B_Z was mostly negative during the selected intervals (IMF B_Z was negative for more than 90% of an event duration for more than 90% of events). This value is somewhat lower for DeJong list.

Figures 1c and 1d show the histograms of the IMF B_Z and solar wind electric field averaged over the SMC event duration. It can be seen that for most of events $B_Z > -5$ nT and it is in rough agreement with the threshold for the balanced-reconnection intervals obtained by *Tanskanen et al.* [2005]. The histograms also show that there are more active events in the DeJong's list. According to *DeJong* [2014], other selection procedures tend to miss the SMC events during high magnetospheric activity intervals. The Kissinger list contains the largest number of events with weak solar wind driving. It is due to the fact that *Kissinger et al.* [2011] procedure sets $AL = -75$ nT as a lower threshold of activity while *Juusola et al.* [2013] require $AL < -130$ nT.

To get an idea of how close these lists are to each other, we check the intervals when these lists overlap. Table 2 shows the percentage of the time when the events selected by different criteria are overlapped. For each pair of selection criteria (left and right columns of Table 2), we summed the time intervals which belong to both lists. The numbers on the left (right) side from the /-sign in the middle column shows this time as a percentage

of total SMC events duration in the list specified in the left (right) column. It can be noted that although the characteristics of the Kissinger and Juusola event lists are almost identical, it is only for 50% of SMC duration that Juusola SMCs overlap with Kissinger ones.

Although the presented analysis has revealed the serious problems in the methods of SMC selections, the rating of these criteria or the elaboration of the new one is out of the scope of this study. For this reason, we conducted an analysis for all three list of SMC events to see if the results are different for the different selections.

3. Ring current intensity estimation

In order to estimate the symmetric ring current intensity, we use the so called “event-oriented” modeling approach. The idea of the method is to fine-tune a standard empirical model to achieve a better agreement with the observations during the event of interest [e.g., *Pulkkinen et al.*, 1991; *Sergeev et al.*, 1994; *Kubyshkina et al.*, 1999; *Ganushkina et al.*, 2004, 2010]. Usually, the standard model is slightly modified and a few free parameters are introduced (e.g. current system intensities, geometry parameters). These parameters can be totally new or the standard model coefficients can be treated as free parameters. These parameters are found minimizing the difference between the model and observations during the event of interest. Generally, this approach requires a few spacecraft properly positioned in the region of interest (see *Kubyshkina et al.* [2009] to find more details). However, good spacecraft constellations are rare and to obtain large statistics we adapted this method to the single spacecraft observation. This limitation reduces the method accuracy but increases the number of events suitable for modeling.

We use two empirical models referred to as T01 [*Tsyganenko, 2002a, b*] and TS05 [*Tsyganenko and Sitnov, 2005*]. Their field is represented as a sum of several terms.

$$\mathbf{B}(\mathbf{r}, \tilde{P}) = \sum_i A_i \mathbf{b}_i(\mathbf{r}, C_{i1}, C_{i2}, \dots) \quad (1)$$

Here, \mathbf{r} is the position vector and \tilde{P} is the vector of the model input parameters (these parameters are solar wind parameters and indices of geomagnetic activity). Each term represents one of the conventional current systems, for example Symmetric Ring Current (SRC), tail current, etc. The field corresponding to each system is computed as a product of scalar function A_i and vector function \mathbf{b}_i . The vector functions depend also on several nonlinear parameters C_{ij} which define the current system geometry. Both A and C_{ij} are functions of the model input parameters \tilde{P} ($A_i = A_i(\tilde{P})$, $C_{ij} = C_{ij}(\tilde{P})$).

All vector functions \mathbf{b}_i have zero normal component on the magnetopause. For this reason, the scalar coefficients can be varied arbitrarily, the model field stays shielded inside magnetosphere. It should be noted that although Equation (1) looks as an expansion into the basis vectors, neither \mathbf{b}_i are unit length vectors nor the current of corresponding current systems is a unit current.

For a given current system geometry, A_i is proportional to the total current system intensity. Having a single spacecraft observation we can introduce only one free parameter. Since we are interested in the ring current strength, we treat the model coefficient A_{SRC} as a free parameter a . All other current systems as well as the vector function for the field of the SRC module remain unchanged.

$$\mathbf{B}^{mod} = a\mathbf{b}_{SRC} + \mathbf{B}_{other}^{mod} \quad (2)$$

Here, \mathbf{B}_{other}^{mod} is the sum of the magnetic fields of all model systems except for SRC. The free parameter can be determined by minimization of the difference between model and observation $\Delta(a) = (\mathbf{B}^{obs} - \mathbf{B}^{mod})^2$.

$$a = \mathbf{b}_{SRC} \cdot (\mathbf{B}^{obs} - \mathbf{B}_{other}^{mod}) / b_{SRC}^2 \quad (3)$$

Obviously, this method can give us a correct estimate for ring current intensity only if the standard model gives correct fields for all other sources, and the geometry of the real SRC is the same as in the model SRC module. Let us assume that we can separate the real magnetospheric current systems into a symmetric one (flowing around the Earth) and all other systems (see *Liemohn et al.* [2011] and *Ganushkina et al.* [2012] on the uncertainty of such separation). Figure 2a shows schematically the magnetic field vectors of the model (black) and real (red) current systems. Here we assume that the real vectors have the same orientation as the model ones but different magnitude. After expansion of the dot-product Equation (3) becomes:

$$a = \frac{B_{SRC}^{obs}}{b_{SRC}} + \frac{(B_{other}^{obs} - B_{other}^{mod})}{b_{SRC}} \cos \delta \quad (4)$$

The first term on the right side is the correct value of the ring current system intensity estimation and the second term is the error (because the model gives a wrong value for B_{other}^{mod}). The effect of the uncertainty in the B_{other} can be minimized if \mathbf{b}_{SRC} is perpendicular to \mathbf{B}_{other}^{mod} ($\delta = 90^\circ$, Figure 2b).

However, even if the aforementioned condition is fulfilled, the real SRC field is not necessarily perpendicular to real field from all other sources. The realistic configuration is shown in Figure 2c. In such a case, Equation (3) becomes:

$$a = \frac{B_{SRC}^{obs}}{b_{SRC}} \cos \beta + \frac{B_{other}^{obs}}{b_{SRC}} \sin \alpha \quad (5)$$

Let us assume that $a_{true} = B_{SRC}^{obs}/b_{SRC}$ gives the correct estimate of the SRC intensity.

Then, the estimation for the relative error is:

$$(a - a_{true})/a_{true} = \cos \beta - 1 + \frac{B_{other}^{obs}}{B_{SRC}^{obs}} \sin \alpha \quad (6)$$

It can be seen that the accuracy of the method is higher if β and α are closer to zero and the measurements are made in the region where the magnetic field of the ring current is stronger than the field from all other systems. For $\beta = 10^\circ$, $\alpha = 30^\circ$, and $B_{SRC}^{obs} = 2B_{other}^{obs}$, Equation (6) gives $\Delta a/a = 27\%$. Here, we assume that the model reproduces better the orientation of the ring current magnetic field than the magnetic field of all other systems. It is justified because the ring current flows in the region of the strong and stable dipole field.

We use these conditions as the criteria for selection of the region where spacecraft magnetic field observations can be used as an input for our method. First, we need to find the region where the ratio B_{SRC}/B_{other} is maximal. We cannot do it explicitly (or using a standard model) because we do not know the real B_{SRC} or B_{other} . However, the regions as far as possible from the tail current as well as magnetopause currents and partial ring current are likely to be the best choice. The subtraction of the Earth's internal

magnetic field from the measurements in the close-to-Earth vicinity is problematic. For this reason we do not use the observations at $r < 3R_E$. We selected the observations on the dayside between 8 and 12h MLT.

In addition, we select the observations where model \mathbf{B}_{SRC} is perpendicular to the model \mathbf{B}_{other} within $\pm 10^\circ$ margin. Figure 3 shows the T01 model magnetic field vectors on the dayside in the XZ GSM plane for the model parameters typical for the SMC periods ($P_d = 1.65$ nPa, $Dst = -20$ nT, IMF $B_Z = -2.6$ nT, $G_1 = 3.96$, $G_2 = 5.63$). Figure 3a and 3b show the magnetic field of the SRC module and field of all other systems, respectively. Figure 3c shows both vectors in the points where $\mathbf{B}_{SRC} \perp \mathbf{B}_{other}$ within a $\pm 10^\circ$ margin. It can be seen that there are two branches of points. This pattern is also reproduced for the TS05 model. We discard the points on the right branch because they are too close to the magnetopause currents. We have experimented with the T01 and TS05 models varying the Earth's dipole tilt angle and solar wind dynamic pressure and found that this branch can be excluded using conditions $r \leq 6.6R_E$ and $X^2 + Y^2 \leq (Z/0.436)^2 + 25$ computed in the Solar-Magnetospheric (SM) system (all variables are in earth's radii).

Although Figure 3c gives an impression that the selected region is rather narrow and the chance for spacecraft to be there during an SMC event is low, it is not true because the width of that region increases towards the dawn flanks.

The magnetospheric cusp diamagnetic currents are not included in the models. At the same time, they cause a prominent depression of the magnetic field inside the cusp region [Tsyganenko, 2009]. For this reason, we use the empirical equation for the latitude of the cusp equatorial boundary [Newell et al., 2006] to exclude the measurements which could be affected by the cusp currents.

$$|\Lambda_c| = 78.5^\circ - 2.27 \cdot 10^{-3} E_{WAV} \pm 0.03 \Psi$$

$$E_{WAV} = V B_T \sin^4(\theta/2) \quad (7)$$

Here, Ψ is the Earth dipole tilt angle (in degrees, we use the plus and minus signs for the cusps in the north and south hemispheres, respectively). V and B_T are the solar wind flow velocity and transverse component of IMF (units are km/s and nT), and θ is the IMF clock angle.

We require that the projection of the spacecraft (using the standard model) is at least 2° to the equator from the predicted cusp equatorial boundary. This requirement also ensures that the spacecraft is not in the field-aligned current region. The field-aligned currents are very volatile systems which are reproduced by the model only in a statistical sense [Dubyagin et al., 2014]. For this reason, their contribution can be confused with the SRC field. In addition, Figure 3c clearly shows that the B_{other}/B_{SRC} ratio increases with distance from the equatorial plane and, hence, accuracy of our method decreases at high latitudes.

It should be noted that all aforementioned criteria are checked using the standard model (T01 or TS05) with the input parameters corresponding to the modelled time. On the other hand, the result of the check could be different if the modified model (fitted to observations) were used. In this study we neglect this difference since we perform our analysis for numerous events, and also validate our method in Section 5. To make sure that our results are not influenced by the choice of a particular model, we perform our analysis for two models.

4. Data

As input for our ring current intensity determination method, we use magnetic field measurements onboard the Time History of Events and Macroscale Interactions during Substorms (THEMIS), Cluster, and Polar spacecraft. The THEMIS flux-gate magnetometer (FGM) data were downloaded and calibrated using software from <http://themis.ssl.berkeley.edu/index.shtml>. The data cover the interval May, 2007 – May, 2013. The spin-resolution data of FGM [Balogh *et al.*, 2001] on board the four Cluster satellites were downloaded from the Cluster Active Archive (<http://caa.estec.esa.int>). These data cover the interval October, 2001 – August, 2013. The spin resolution data of the Polar Magnetic Field Experiment [Russell *et al.*, 1995] were downloaded from www-ssc.igpp.ucla.edu/forms/polar/. These data cover the interval October, 1996 – March, 2008. The International Geomagnetic Reference Field was subtracted from the spin resolution data. After that, the magnetic field measurements were averaged over 5 min. The input parameters for the T01 model as well as the estimates of the magnetosphere driving parameters were computed using the solar wind and IMF parameters at 1 min and 5 min resolution from the OMNI database from the GSFC/SPDF OMNIWeb interface at <http://omniweb.gsfc.nasa.gov>. The SYM-H and auroral electrojet indices were downloaded from the World Data Center for geomagnetism, Kyoto (<http://wdc.kugi.kyoto-u.ac.jp/>). The input parameters for the TS05 model were taken from http://geo.phys.spbu.ru/~tsyganenko/TS05_data_and_stuff/.

5. Validation of the method

Since the method's accuracy critically depends on a number of assumptions, it should be tested. For this purpose, we need to choose the events when the ring current intensity is

known. It is generally agreed that during the recovery phase of the storms the symmetric ring current makes the dominant contribution to the SYM-H index [e.g. *Liemohn et al.*, 2001b; *Ganushkina et al.*, 2004; *Tsyganenko and Sitnov*, 2005]. It is also obvious that the ring current is rather weak if conditions are totally quiet for a long period of time. In this section, we compare the real SYM-H index with the contribution to the SYM-H index from the model SRC (with intensity value obtained from our method). We selected periods during recovery phases of the storms with the peak SYM-H < -50 nT (the recovery phase is defined as a period after SYM-H peak until SYM-H attains -10 nT). To exclude the periods of transient storm intensification during recovery phase, we also required that IMF B_Z was positive for 30 minutes prior to observation. We also selected quiet periods with AE < 50 nT and SYM-H > -5 nT for 2 hours prior to observation.

After such intervals were selected, as well as for the lists of SMC events, we checked if the Cluster, THEMIS or Polar spacecraft were in the region where our method could be applied (see Section 3). We made sure that the input parameters for the T01 or TS05 were available and that the model B_{SRC} was nearly perpendicular to the model B_{other} (see Section 3). If all criteria were fulfilled, we fitted the model to the observations and obtained the SRC amplitude.

Figure 4 shows the positions of the spacecraft in the SM coordinates when their measurements were used for the SRC amplitude determination. Red and black symbols correspond to the storm recovery and quiet periods, respectively. Other colors correspond to the SMC events (see graph legend). Left and right columns of the figure correspond to the T01 and TS05 models, respectively.

Having the value of the ring current amplitude, we computed the ring current contribution to the SYM-H index. The detailed procedure for the estimation of the contribution to SYM-H from particular current systems can be found in *Dubyagin et al.* [2014]. In brief, the ring current contribution to SYM-H is computed using a procedure which is equivalent to that for the real SYM-H index. We compute the H-component of the model field at the six observatories on the ground. Then, we subtract a quiet time baseline (in our case it is the field of the standard model with the input parameters typical for the most quiet days). However, instead of the total model field, we only use the SRC term.

We use the equation from *Burton et al.* [1975] for removal of the magnetopause current contribution as well as the quiet time baseline from the SYM-H index:

$$\text{SYM-H}^* = \text{SYM-H} - 15.8\sqrt{P_d} + 20 \text{ nT} \quad (8)$$

Here, SYM-H* is the corrected index in nanoteslas and P_d is the dynamic pressure of the solar wind in nanopascals.

Figure 5 shows SYM-H* versus model SRC contribution to SYM-H. The black and red symbols correspond to the values obtained using the T01 and TS05 models (as a basis for our method except for Figure 5b where the standard models were used), respectively. Since the number of data points when model input parameters are available is generally higher for the T01 model, the results obtained by using TS05 are represented by fewer points in Figure 5. The model SRC contribution to SYM-H is divided by 0.8 to take into account the contribution from the current induced in the ground [*Häkkinen et al.*, 2002]. Figure 5a shows the result obtained using our method for a recovery phase. The points on the diagonal line correspond to 100% SRC contribution to SYM-H. It can be seen that

the points are scattered around this diagonal line as it can be expected for a recovery phase.

To evaluate how our method works in comparison to the original Tsyganenko models, we computed the same values as in Figure 5a but using the standard (unmodified) T01 and TS05 models. These results are shown in Figure 5b. It can be seen that although the scatter for each model is somewhat smaller than that for our method, the two models show very different results. This figure reflects the well-known fact that although both models generally reproduce the observed SYM-H index very well, the relative contribution of the SRC and cross-tail current modules in these models is dramatically different [Dubyagin *et al.*, 2014]. In fact, the SRC amplitude in the T01 model is parameterized by only two parameters, SYM-H and solar wind dynamic pressure, for this reason the scatter for the T01 model in Figure 5b is due to the P_d variation. For the same reason, the model cannot distinguish between the main and recovery phases. The TS05 model shows more reasonable results (that seems natural, since it was designed to describe the storm-time magnetosphere). It is worth noting that our method equalizes the difference between the models at least for the moderate SYM-H values. It can be seen that all red points in Figure 5b lie above the diagonal while they are rather scattered around the diagonal in Figure 5a. Although the TS05 parametrization cannot distinguish the main and recovery phases and the SRC contribution can be underestimated for some points in Figure 5b, it might also mean that our method slightly overestimates the SRC intensity.

Figure 5c shows the result obtained using our method for quiet conditions in the same format. It can be seen that SRC makes very small or event positive contribution to SYM-H. The positive values of SRC contribution should be explained. It can be a result of

the subtraction of the quiet-time baseline if the SRC intensity obtained by our method is lower than the SRC intensity of the standard model for nominal quiet-time parameters. In addition, Equation (6) demonstrates that the relative error of our method is large when SRC is weak. Apparently our method systematically underestimates the SRC intensity in such cases. Sometimes, it even outputs negative values for the SRC intensity. Since such values cannot be real, we set zero SRC intensity for these events. These points create a top cutoff effect at $\sim +15$ nT level seen in Figure 5c.

Finally, we present the results of the intercomparison of the method outputs for the events when a few spacecraft were located in the region of the method applicability. For every event, we define a reference spacecraft as the farthest spacecraft from the Earth. Figure 6 shows the SRC contribution to SYM-H obtained using the measurements at the reference spacecraft versus those whose values are obtained using the measurements at another spacecraft for the same time. The color indicates the distance between the spacecraft. We do not show the points when the distance is less than $0.5R_E$ since they cluster near the diagonal and just demonstrate a good intercalibration of the spacecraft magnetometers. It can be seen that the method outputs obtained using different spacecraft data are mostly identical within a margin of 10 nT (with one exception ~ 13 nT).

Obviously such a simple method cannot be very accurate, but the error is likely $\leq 30\%$ or ≤ 15 nT. This is only a little higher than the 20% error between global low-latitude magnetic perturbation indices during active times [*Katus and Liemohn, 2013*]. Such accuracy is enough to distinguish the cases when SRC is strong or weak.

6. Application of method to SMCs

Figure 7 shows the result of the application of our method to SMC events in the same format as in Figure 5. Figures 7a, 7b, and 7c correspond to results for the Kissinger, Juusola, and DeJong lists of SMC events, respectively. Black and red colors correspond to the results obtained using the T01 and TS05 models, respectively. Since we use 5 minute resolution and several spacecraft, most of the SMC events from our lists are represented by a number of points corresponding to the several 5 minute measurements during single SMC event or to the simultaneous measurements at several spacecraft. The legends show the number of the individual SMC events represented in each figure. Both models give similar results. For the majority of events, SYM-H* was rather moderate (> -40 nT). For this range of SYM-H*, all three selections of the SMC events show similar results. The SRC contribution to SYM-H varies for different events from 0 to 100% (our method becomes inaccurate if SRC is weak). There are very few points for SYM-H* < -40 nT in Figures 7a and 7b. Two points in Figure 7a correspond to very small contribution of SRC to SYM-H while a few points in Figure 7b are near the diagonal line. This discrepancy is likely just a result of a small number of events in the Kissinger and Juusola lists rather than the real properties of these data sets. There are many more points in Figure 7c and these points are almost evenly distributed between the diagonal and zero-contribution line for the whole range of SYM-H*.

Although Figure 7 shows that SRC can be weak during the SMC event, it cannot give the definite answer to the question about the role of the ring current in stabilizing the magnetotail current during SMCs, since there is no information about solar wind driving for the events with a small SRC contribution. If the driving was weak for these events, a strong ring current would not be needed for supporting magnetotail stability.

We use the *Boyle et al.* [1997] empirical equation for the polar cap potential as a parameter quantifying the rate of the magnetic flux reconnection at the dayside magnetopause.

$$\Phi_{PC} = 10^{-4}V^2 + 11.7B \sin^3 \frac{\phi}{2} \quad (9)$$

Here, $\phi = \arccos(B_Z/B)$, B is the magnitude of IMF in nanoteslas and V is the solar wind flow velocity in km/s. For every SMC event we computed the mean of the Φ_{PC} over the whole SMC event duration except for the first and last half an hour (to avoid the possible influence of the leading and trailing substorms). We also required that there were no gaps in the solar wind data longer than 10 min. The last requirements significantly reduced the number of points. However, even for the worst data set (T01 for Juusola list), we still have 18 SMC events represented in Figure 8b.

Figure 8 shows the contribution of the SRC to the SYM-H versus mean polar cap potential. Panels (a), (b), and (c) correspond to the Kissinger, Juusola, and DeJong data sets, respectively. A very weak dependence of SRC strength on $\langle \Phi_{PC} \rangle$ can be seen mostly for the low envelope of the cloud of the points. This dependence probably just reflects the statistical relation between the ring current strength and solar wind driving. *O'Brien et al.* [2002] reported that typical IMF B_Z is ~ 3 nT and velocity is below 450 km/s during SMC events. For such parameters, Equation (9) gives $\Phi_{PC} = 55$ kV and we consider the events with $\langle \Phi_{PC} \rangle$ above this threshold as events with strong driving. It can be seen, that even for events with $\langle \Phi_{PC} \rangle > 70$ kV, the SRC contribution to SYM-H can be rather weak (> -10 nT).

However, there are quite few points in Figure 8. As an additional test, in Figure 9 we plot the minimum SYM-H* versus $\langle \Phi_{PC} \rangle$ for the whole list of the SMC events. Figures

9a and 9b correspond to the Juusola and DeJong list of SMCs, respectively. Almost no dependence is seen in 9a and very weak dependence can be seen for DeJong SMCs, mostly for very strong solar wind driving. In contrast to Figure 8, here we do not know what part of the SYM-H* is caused by SRC. The dependence seen in Figure 9b can be caused by the cross-tail current which responds to the stronger solar wind driving. We also tried to use the *Newell et al.* [2007] “universal” coupling function instead of the polar cap potential and also tried different combinations of the peak and average values of the parameters (e.g. $\langle \text{SYM-H}^* \rangle$ versus $\max \Phi_{PC}$) but the results were always similar (not shown).

7. Discussion

Juusola et al. [2013] have published results supporting the hypothesis that the enhanced ring current can be the main cause of the magnetosphere stability during the steady magnetospheric convection events. In order to check this hypothesis, we developed a method of estimation of the symmetric ring current strength from the single spacecraft observations. We used three different automatic selection criteria, adopted from the literature [*Kissinger et al.*, 2011; *Juusola et al.*, 2013; *DeJong*, 2014], to select the SMC events. All these criteria used the auroral electrojet indices for selection of the intervals of the enhanced convection with no substorm signatures. We have found that these procedures select rather different sets of events (see Section 2) with a maximum time overlap between them $\sim 60\%$. The selection quality can be affected by imperfections of the auroral electrojet indices which are known to have some limitations [*Akasofu et al.*, 1983; *Sergeev et al.*, 2014]. However, *McPherron et al.* [2005] found that occurrence of SMCs selected using the AE index does not depend on universal time, demonstrating that uneven and

rather sparse distribution of the ground observatories over the local time has no effect on the SMC selection.

Two of the aforementioned selection procedures (Kissinger and Juusola) select mostly rather short intervals $\sim 1.5\text{--}2$ h (see Figure 1a). *Sergeev et al.* [2001] discriminated between the longer lasting SMC events and shorter duration (1–2 substorm time-scale) convection bay events. According to the authors, the large-scale magnetospheric configuration is not stationary during the convection bays. *Pulkkinen et al.* [2013] carried out their analysis for the *Kissinger et al.* [2011] SMC list and found that their SMCs remind them of a weak and prolonged growth phase (the magnetosphere configuration was not stationary but changed slowly).

The SMC events are the intervals of the balanced reconnection in the distant tail and on the dayside magnetopause [*Dmitrieva et al.*, 2004], and the classic definition of SMC requires that IMF was southward and stable [*Sergeev et al.*, 1996]. Figure 1b demonstrated that not all events in our lists were accompanied by purely negative IMF B_z . That is, some events from our list are not SMCs in a strict sense.

The original *DeJong* [2014] algorithm of the SMC selection includes visual inspections of the spectrograms obtained by Los Alamos National Laboratory (LANL) geosynchronous spacecraft. The injections were considered to be signatures of substorms and those events were discarded. According to the authors, this procedure removes 15% of events from the automatically generated list. In the present study, we did not apply any visual inspections. Although the injections at geosynchronous orbit are typically observed during the substorms [*Arnoldy and Chan*, 1969; *Baker et al.*, 1982], it does not mean that they could not be produced by the Bursty Bulk Flows (BBFs) [*Angelopoulos et al.*, 1992] without a

substorm. Multiple BBFs are observed in the magnetotail during the SMCs [e.g. *Kissinger et al.*, 2012; *Pulkkinen et al.*, 2013]. The sudden increase of the particle fluxes (particle injection) is observed when BBF passes by a spacecraft in the mid- and near-earth tail [*Gabrielse et al.*, 2014] and it also can cause the injection at geosynchronous orbit. For example, *Sergeev et al.* [2001] reported that soft injections were observed at $r = 6.6R_E$ during the convection bay event. That is, some of the injections at LANL spacecraft can be related to BBFs rather than a substorm. For this reason, we argue that the visual inspection of the spectrograms from the geostationary satellites is not necessary (at least, without taking into account the injection intensity).

Nakai and Kamide [2003] and *Milan et al.* [2009] showed that the threshold magnitude of the lobe magnetic flux, above which the substorm onset is favored, depends on the SYM-H (or Dst) index. The authors speculated that the ring current somehow stabilizes the tail current sheet. *Milan et al.* [2009] proposed a scenario in which the ring current magnetic field penetrates to the mid-tail and increases the normal component in the neutral sheet. Although the experimental results of these studies are robust and solid, the application of the proposed scenario to the SMC periods is questionable. It has been shown that the magnetic configuration during an SMC has a region of the weak B_Z in the near-earth tail and a region of large B_Z in the mid-tail [*Sergeev et al.*, 1994, 2001]. Obviously, according to *Milan et al.* [2009] scenario, the ring current would produce even stronger B_Z in the near-Earth tail than in the mid-tail. On the other hand, intense cross-tail current or partial ring current in the near-earth region produces positive B_Z downtail. Moreover, the cross-tail current gives significant contribution to the SYM-H depression during the main phase of the geomagnetic storm [*Turner et al.*, 2000; *Ganushkina et al.*, 2004; *Maltsev,*

2004; *Ganushkina et al.*, 2010]. This could happen also during the non-storm SMC events. *Shukhtina et al.* [2005] found that the tail magnetic flux accumulated by the end of the growth phase depends mainly on the merging electric field with correlation coefficient 0.95. Such high correlation implies that the dependence on Dst found by *Nakai and Kamide* [2003] and *Milan et al.* [2009] is due to the fact that merging electric field is usually higher during strong storms.

We estimated the SRC contribution to SYM-H index for a number of SMC events and found almost continuous distribution from 100% to 0% contribution. *Milan et al.* [2009] and *Juusola et al.* [2013] scenarios imply that the stronger solar wind driving is, the stronger ring current needed to support the magnetotail stability. However, we could not find any significant dependence of the SRC intensity on the solar wind driving strength (see Section 6). Although we tested our method in Section 5, we cannot rule out the possibility that the method can give incorrect values for some events because the tests were carried out for the northward IMF B_Z , while during SMC events, IMF B_Z is mostly negative. For this reason, we also use the SYM-H* as a proxy of the ring current strength (see Figure 9), and again we did not find any significant correlation between the SYM-H* and solar wind driving during the SMC events. This findings imply that the symmetric ring current does not affect the magnetotail stability during the steady magnetospheric convection intervals.

Note that this study only investigated a single free parameter, the intensity of the symmetric ring current, in the T01 and TS05 magnetic field models. Other variables related to the SRC were not changed in an event-oriented fitting procedure. Specifically, we did not vary the radial location or radial spread of the SRC in the models. It could

be that during the relatively weak driving of SMCs, a symmetric ring current forms either farther out from the Earth or across a broader extent in L value. Furthermore, we only tested the symmetric ring current and not the partial ring current in the models. This other near-Earth current system could still be performing the stabilization process speculated by *Milan et al.* [2009]. Several numerical modeling studies have found an inflated tail field in the presence of a strong inner magnetospheric pressure, which is usually not symmetric but rather localized at midnight in a partial ring current configuration [e.g. *De Zeeuw et al.*, 2004; *Ridley et al.*, 2010; *Welling and Ridley*, 2010].

Finally, the very name of SMC implies continuous flow through the magnetosphere. Therefore, it could be that development of a symmetric ring current is systematically suppressed during SMCs. Indeed, numerous studies have shown that the symmetric ring current is rather weak during intervals southward IMF (i.e., storm main phases) [e.g. *Alexeev et al.*, 1996; *Turner et al.*, 2000; *Liemohn et al.*, 2001a, b; *Maltsev*, 2004; *Ganushkina et al.*, 2004; *Kalegaev et al.*, 2005; *Ganushkina et al.*, 2010], and the IMF during SMCs is typically southward. Our findings here support this conclusion that the symmetric ring current is a minor contributor to the SYM-H index during SMCs.

8. Conclusion

Using the spacecraft magnetic field measurements we have estimated the symmetric ring current intensity during numerous SMC events. Analyzing these data together with the concurrent solar wind parameters, we conclude that there is no causal relationship between the symmetric ring current strength and the magnetotail stability during the SMC intervals.

Acknowledgments. The authors thank Dr. V. Sergeev for reading the manuscript and his thoughtful comments. The work by SD and part of work by NG was supported by Academy of Finland. The work was supported in the USA by NASA grants NNX11AO60G and NNX14AC02G. The work by MK was supported by RF president grant #2836.2014.5. The part of the research leading to these results has received funding from the European Union Seventh Framework Programme (FP7/2007-2013) under grant agreements No 606716 SPACESTORM and from the European Unions Horizon 2020 research and innovation programme under grant agreement No 637302 PROGRESS. N. Ganushkina thanks the International Space Science Institute in Bern, Switzerland, for their support of the international teams on Analysis of Cluster Inner Magnetosphere Campaign data, in application the dynamics of waves and wave-particle interaction within the outer radiation belt and "Ring current modeling: Uncommon Assumptions and Common Misconceptions". The work of N. Ganushkina was also partly supported by NASA award NNX14AF34G. The data of the magnetometer on board Cluster satellites were downloaded from the Active Cluster Archive (<http://caa.estec.esa.int>). The data of the Polar Magnetic Field Experiment were downloaded from www-ssc.igpp.ucla.edu/forms/polar/. The authors acknowledge the Kyoto World Data Center for Geomagnetism (<http://wdc.kugi.kyoto-u.ac.jp/>). The authors also acknowledge use of NASA/GSFC's Space Physics Data Facility's OMNIWeb service, and OMNI data (<http://omniweb.gsfc.nasa.gov>). Thanks to K. H. Glassmeier, U. Auster, and W. Baumjohann for the use of THEMIS FGM data provided under the lead of the Technical University of Braunschweig and with financial support through the German Ministry for Economy and Technology and the German Center for Aviation and Space (DLR) under contract 50 OC 0302.

References

- Akasofu, S.-I., B.-H. Ahn, Y. Kamide, and J. H. Allen (1983), A note on the accuracy of the auroral electrojet indices, *J. Geophys. Res.*, *88(A7)*, 5769-5772, doi:10.1029/JA088iA07p05769.
- Alexeev, I. I., E. S. Belenkaya, V. V. Kalegaev, Y. I. Feldstein, and A. Grafe (1996), Magnetic storms and magnetotail currents, *J. Geophys. Res.*, *101(A4)*, 7737-7747, doi:10.1029/95JA03509.
- Angelopoulos, V., W. Baumjohann, C. Kennel, F. Coroniti, M. Kivelson, R. Pellat, R. Walker, H. Lühr, and G. Paschmann (1992), Bursty Bulk Flows in the Inner Central Plasma Sheet, *J. Geophys. Res.*, *97(A4)*, 4027-4039.
- Arnoldy, R. L., and K. W. Chan (1969), Particle substorms observed at the geostationary orbit, *J. Geophys. Res.*, *74(21)*, 5019-5028, doi:10.1029/JA074i021p05019.
- Baker, D. N., et al. (1982), Observation and modeling of energetic particles at synchronous orbit on July 29, 1977, *J. Geophys. Res.*, *87(A8)*, 5917-5932, doi:10.1029/JA087iA08p05917.
- Balogh, A., et al. (2001), The Cluster Magnetic Field Investigation: overview of in-flight performance and initial results, *Ann. Geophys.*, *19*, 1207-1217, doi:10.5194/angeo-19-1207-2001.
- Boyle, C. B., P. H. Reiff, and M. R. Hairston (1997), Empirical polar cap potentials, *J. Geophys. Res.*, *102(A1)*, 111-125, doi:10.1029/96JA01742.
- Brittnacher, M., K. B. Quest, and H. Karimabadi, (1994), On the energy principle and ion tearing in the magnetotail, *Geophys. Res. Lett.*, *21*, 1591-1594, doi:10.1029/94GL01697.

- Burton, R. K., R. L. McPherron, and C. T. Russell (1975), An empirical relationship between interplanetary conditions and Dst, *J. Geophys. Res.*, *80(31)*, 4204-4214, doi:10.1029/JA080i031p04204.
- DeJong, A. D., and C. R. Clauer (2005), Polar UVI images to study steady magnetospheric convection events: Initial results, *Geophys. Res. Lett.*, *32*, L24101, doi:10.1029/2005GL024498.
- DeJong, A. D. (2014), Steady magnetospheric convection events: How much does steadiness matter?, *J. Geophys. Res. Space Physics*, *119*, 4389-4399, doi:10.1002/2013JA019220.
- De Zeeuw, D. L., S. Sazykin, R. A. Wolf, T. I. Gombosi, A. J. Ridley, and G. Tóth (2004), Coupling of a global MHD code and an inner magnetosphere model: Initial results, *J. Geophys. Res.*, *109*, A12219, doi:10.1029/2003JA010366.
- Dmitrieva, N. P., Sergeev, V. A., and Shukhtina, M. A.: Average characteristics of the midtail plasma sheet in different dynamic regimes of the magnetosphere, *Ann. Geophys.*, *22*, 2107–2113, doi:10.5194/angeo-22-2107-2004, 2004.
- Dubyagin, S., N. Ganushkina, M. Kubyshkina, and M. Liemohn (2014), Contribution from different current systems to SYM and ASY midlatitude indices, *J. Geophys. Res. Space Physics*, *119*, 7243-7263, doi:10.1002/2014JA020122.
- Gabrielse, C., V. Angelopoulos, A. Runov, and D. L. Turner (2014), Statistical characteristics of particle injections throughout the equatorial magnetotail, *J. Geophys. Res. Space Physics*, *119*, 2512-2535, doi:10.1002/2013JA019638.
- Ganushkina, N. Yu., Pulkkinen, T. I., Kubyshkina, M. V., Singer, H. J., and Russell, C. T.: Long-term evolution of magnetospheric current systems during storms, *Ann.*

Geophys., *22*, 1317–1334, doi:10.5194/angeo-22-1317-2004, 2004.

Ganushkina, N. Yu., Liemohn, M. W., Kubyshkina, M. V., Ilie, R., and Singer, H. J.: Distortions of the magnetic field by storm-time current systems in Earth's magnetosphere,

Ann. Geophys., *28*, 123–140, doi:10.5194/angeo-28-123-2010, 2010.

Ganushkina, N. Y., S. Dubyagin, M. Kubyshkina, M. Liemohn, and A. Runov (2012), Inner magnetosphere currents during the CIR/HSS storm on July 21-23, 2009, *J. Geophys. Res.*,

117, A00L04, doi:10.1029/2011JA017393.

Ganushkina, N. Y., et al. (2015), Defining and resolving current systems in geospace, *Ann. Geophys.*, accepted.

Häkkinen, L. V. T., T. I. Pulkkinen, H. Nevanlinna, R. J. Pirjola, and E. I. Tanskanen, Effects of induced currents on Dst and on magnetic variations at midlatitude stations,

J. Geophys. Res., *107*(A1), doi:10.1029/2001JA900130, 2002.

Juusola L., N. Partamies, and E. Tanskanen (2013), Effect of the ring current on preconditioning the magnetosphere for steady magnetospheric convection, *Geophys. Res. Lett.*,

40, 1917-1921, doi:10.1002/grl.50405.

Kalegaev, V. V., Ganushkina, N. Y., Pulkkinen, T. I., Kubyshkina, M. V., Singer, H. J., and Russell, C. T.: Relation between the ring current and the tail current during magnetic storms, *Ann. Geophys.*, *23*, 523–533, doi:10.5194/angeo-23-523-2005, 2005.

Katus, R. M., and M. W. Liemohn (2013), Similarities and differences in low- to middle-latitude geomagnetic indices, *J. Geophys. Res. Space Physics*, *118*, 5149-5156, doi:10.1002/jgra.50501.

Kissinger, J., R. L. McPherron, T.-S. Hsu, and V. Angelopoulos (2011), Steady magnetospheric convection and stream interfaces: Relationship over a solar cycle, *J. Geophys.*

Res., 116, A00I19, doi:10.1029/2010JA015763.

Kissinger, J., R. L. McPherron, T.-S. Hsu, V. Angelopoulos, and X. Chu (2012), Necessity of substorm expansions in the initiation of steady magnetospheric convection, *Geophys. Res. Lett.*, 39, L15105, doi:10.1029/2012GL052599.

Kubyschkina, M. V., V. A. Sergeev, and T. I. Pulkkinen (1999), Hybrid Input Algorithm: An event-oriented magnetospheric model, *J. Geophys. Res.*, 104(A11), 24977-24993, doi:10.1029/1999JA900222.

Kubyschkina, M., V. Sergeev, N. Tsyganenko, V. Angelopoulos, A. Runov, H. Singer, K. H. Glassmeier, H. U. Auster, and W. Baumjohann (2009), Toward adapted time-dependent magnetospheric models: A simple approach based on tuning the standard model, *J. Geophys. Res.*, 114, A00C21, doi:10.1029/2008JA013547.

Lembege, B., and R. Pellat (1982), Stability of a thick two-dimensional quasineutral sheet, *Physics of Fluids*, 25, 1995–2004, DOI:10.1063/1.863677.

Liemohn, M. W., J. U. Kozyra, M. F. Thomsen, J. L. Roeder, G. Lu, J. E. Borovsky, and T. E. Cayton (2001a), Dominant role of the asymmetric ring current in producing the stormtime Dst*, *J. Geophys. Res.*, 106(A6), 10883-10904, doi:10.1029/2000JA000326.

Liemohn, M. W., J. U. Kozyra, C. R. Clauer, and A. J. Ridley (2001b), Computational analysis of the near-Earth magnetospheric current system during two-phase decay storms, *J. Geophys. Res.*, 106(A12), 29531-29542, doi:10.1029/2001JA000045.

Liemohn, M. W., D. L. De Zeeuw, R. Ilie, and N. Y. Ganushkina (2011), Deciphering magnetospheric cross-field currents, *Geophys. Res. Lett.*, 38, L20106, doi:10.1029/2011GL049611.

- Maltsev, Y. P. (2004) Points of controversy in the study of magnetic storms, *Space Science Reviews*, *110*(3), 227–267, DOI: 10.1023/B:SPAC.0000023410.77752.30
- McPherron, R. L., T. P. O'Brien, and S. M. Thompson (2005), Solar wind drivers for steady magnetospheric convection, in *Multiscale Coupling of the Sun-Earth Processes*, edited by A. T. Y. Liu, Y. Kamide, and G. Consolini, pp. 113-124, Elsevier, Amsterdam.
- Milan, S. E., Hutchinson, J., Boakes, P. D., and Hubert, B.: Influences on the radius of the auroral oval, *Ann. Geophys.*, *27*, 2913–2924, doi:10.5194/angeo-27-2913-2009, 2009.
- Nakai, H. and Kamide, Y.: Substorm-associated large-scale magnetic field changes in the magnetotail: a prerequisite for "magnetotail deflation" events, *Ann. Geophys.*, *21*, 869–879, doi:10.5194/angeo-21-869-2003, 2003.
- Newell, P. T., T. Sotirelis, K. Liou, C.-I. Meng, and F. J. Rich (2006), Cusp latitude and the optimal solar wind coupling function, *J. Geophys. Res.*, *111*, A09207, doi:10.1029/2006JA011731.
- Newell, P. T., T. Sotirelis, K. Liou, C.-I. Meng, and F. J. Rich (2007), A nearly universal solar wind-magnetosphere coupling function inferred from 10 magnetospheric state variables, *J. Geophys. Res.*, *112*, A01206, doi:10.1029/2006JA012015.
- O'Brien, T. P., S. M. Thompson, and R. L. McPherron, Steady magnetospheric convection: Statistical signatures in the solar wind and AE, *Geophys. Res. Lett.*, *29*(7), doi:10.1029/2001GL014641, 2002.
- T. I. Pulkkinen, D. N. Baker, D. H. Fairfield, R. J. Pellinen, J. S. Murphree, R. D. Elphinstone, R. L. McPherron, J. F. Fennell, R. E. Lopez and T. Nagai (1991), Modeling the growth phase of a substorm using the Tsyganenko Model and multi-spacecraft observations: CDAW-9, *Geophys. Res. Lett.*, *18*, 1963-1966, doi:10.1029/91GL02002.

- Pulkkinen, T. I., N. Partamies, J. Kissinger, R. L. McPherron, K.-H. Glassmeier, and C. Carlson (2013), Plasma sheet magnetic fields and flows during steady magnetospheric convection events, *J. Geophys. Res. Space Physics*, *118*, 6136-6144, doi:10.1002/jgra.50574.
- Ridley, A. J., T. I. Gombosi, I. V. Sokolov, G. Tóth, and D. T. Welling (2010), Numerical considerations in simulating the global magnetosphere, *Ann. Geophys.*, *28*, 1589–1614, doi: 10.5194/angeo-28-1589-2010.
- C. T. Russell, R. C. Snare, J. D. Means, D. Pierce, D. Dearborn, M. Larson, G. Barr, and G. Le (1995), The GGS/POLAR magnetic fields investigation, *Space Sci. Rev.*, *71*, 563–582, doi:10.1007/BF00751341
- Schindler, K. (2007). Physics of space plasma activity, *Cambridge University Press*, ISBN-13 978-0-521-85897-7.
- Sergeev, V. A., T. I. Pulkkinen, R. J. Pellinen, and N. A. Tsyganenko (1994), Hybrid state of the tail magnetic configuration during steady convection events, *J. Geophys. Res.*, *99(A12)*, 23571-23582, doi:10.1029/94JA01980.
- Sergeev V. A., R. J. Pellinen, and T. I. Pulkkinen, Steady magnetospheric convection: A review of recent results, *Space Sci. Rev.*, *75*, 551, 1996
- Sergeev, V. A., M. V. Kubyshkina, K. Liou, P. T. Newell, G. Parks, R. Nakamura, and T. Mukai (2001), Substorm and convection bay compared: Auroral and magnetotail dynamics during convection bay, *J. Geophys. Res.*, *106(A9)*, 18843-18855, doi:10.1029/2000JA900087.
- Sergeev, V. A., D. A. Sormakov, and V. Angelopoulos (2014), A missing variable in solar wind-magnetosphere-ionosphere coupling studies, *Geophys. Res. Lett.*, *41*, 8215-8220,

doi:10.1002/2014GL062271.

- Shukhtina, M. A., N. P. Dmitrieva, N. G. Popova, V. A. Sergeev, A. G. Yahnin, and I. V. Despirak (2005), Observational evidence of the loading-unloading substorm scheme, *Geophys. Res. Lett.*, *32*, L17107, doi:10.1029/2005GL023779.
- Tanskanen, E. I., J. A. Slavin, D. H. Fairfield, D. G. Sibeck, J. Gjerloev, T. Mukai, A. Ieda, and T. Nagai (2005), Magnetotail response to prolonged southward IMF Bz intervals: Loading, unloading, and continuous magnetospheric dissipation, *J. Geophys. Res.*, *110*, A03216, doi:10.1029/2004JA010561.
- Tsyganenko, N. A., A model of the magnetosphere with a dawn-dusk asymmetry, 1, Mathematical structure, *J. Geophys. Res.*, *107(A8)*, doi:10.1029/2001JA000219, 2002.
- Tsyganenko, N. A., A model of the near magnetosphere with a dawn-dusk asymmetry, 2, Parameterization and fitting to observations, *J. Geophys. Res.*, *107(A8)*, doi:10.1029/2001JA000220, 2002.
- Tsyganenko, N. A., and M. I. Sitnov (2005), Modeling the dynamics of the inner magnetosphere during strong geomagnetic storms, *J. Geophys. Res.*, *110*, A03208, doi:10.1029/2004JA010798.
- Tsyganenko, N. A.: Magnetic field and electric currents in the vicinity of polar cusps as inferred from Polar and Cluster data, *Ann. Geophys.*, *27*, 1573–1582, doi:10.5194/angeo-27-1573-2009, 2009.
- Tsyganenko, N. A.: Data-based modelling of the Earth's dynamic magnetosphere: a review, *Ann. Geophys.*, *31*, 1745–1772, doi:10.5194/angeo-31-1745-2013, 2013.
- Turner, N. E., D. N. Baker, T. I. Pulkkinen, and R. L. McPherron (2000), Evaluation of the tail current contribution to Dst, *J. Geophys. Res.*, *105(A3)*, 5431-5439,

Table 1. Total SMC duration for 1996-2013 according to different selection criteria. Last column shows SMC duration as a percentage of time searched.

<i>Juusola et al.</i> [2013]	4332 h	2.7%
<i>Kissinger et al.</i> [2011]	7274 h	4.6%
<i>DeJong</i> [2014]	11814 h	7.5%

Table 2. SMC lists overlap (see explanation in the text).

<i>Kissinger et al.</i> [2011]	34% / 57%	<i>Juusola et al.</i> [2013]
<i>Kissinger et al.</i> [2011]	57% / 35%	<i>DeJong</i> [2014]
<i>DeJong</i> [2014]	22% / 61%	<i>Juusola et al.</i> [2013]

doi:10.1029/1999JA000248.

Welling, D. T., and A. J. Ridley (2010), Validation of SWMF magnetic field and plasma, *Space Weather*, 8, S03002, doi:10.1029/2009SW000494.

Yahnin, A., et al. (1994), Features of steady magnetospheric convection, *J. Geophys. Res.*, 99(A3), 4039-4051, doi:10.1029/93JA02868.

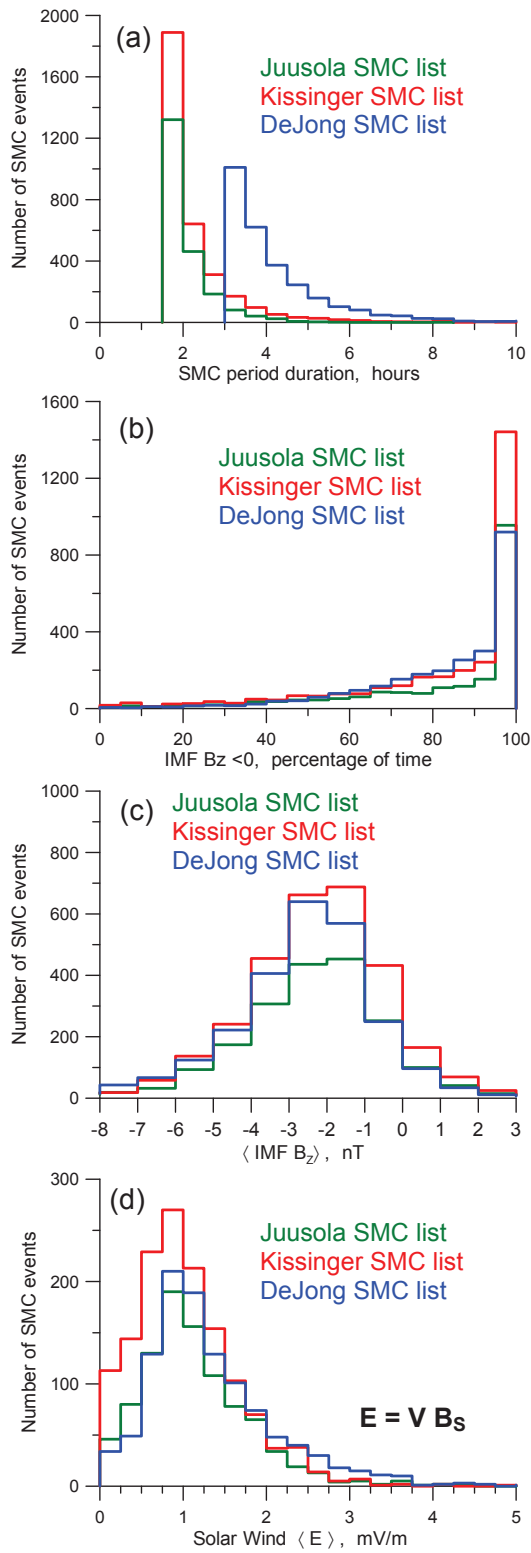


Figure 1. Properties of SMC events for three SMC lists. (a) SMC event duration. (b) Percentage of time when IMF B_z is negative. (c) Mean IMF B_z . (d) Mean solar wind electric field.

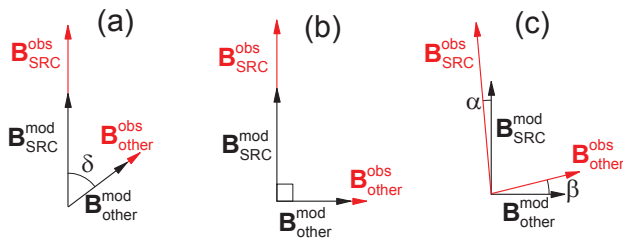


Figure 2. Magnetic field vectors of the model (black) and real (red) current systems. (a) The model SRC field vector is at an angle to the magnetic field from all other model systems. (b) The vectors are perpendicular. (c) Realistic situation: the real vectors are different from the model ones in direction and magnitude.

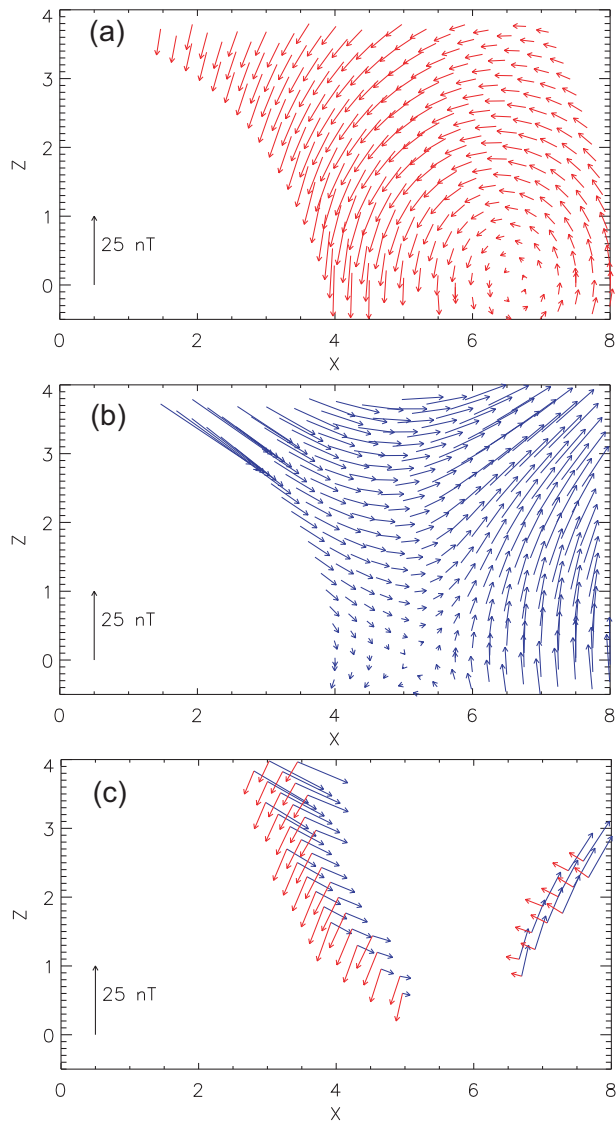


Figure 3. Vectors of T01 magnetic field in XZ GSM plane. (a) SRC field. (b) Field of all systems except for SRC. (c) Only nearly perpendicular vectors.

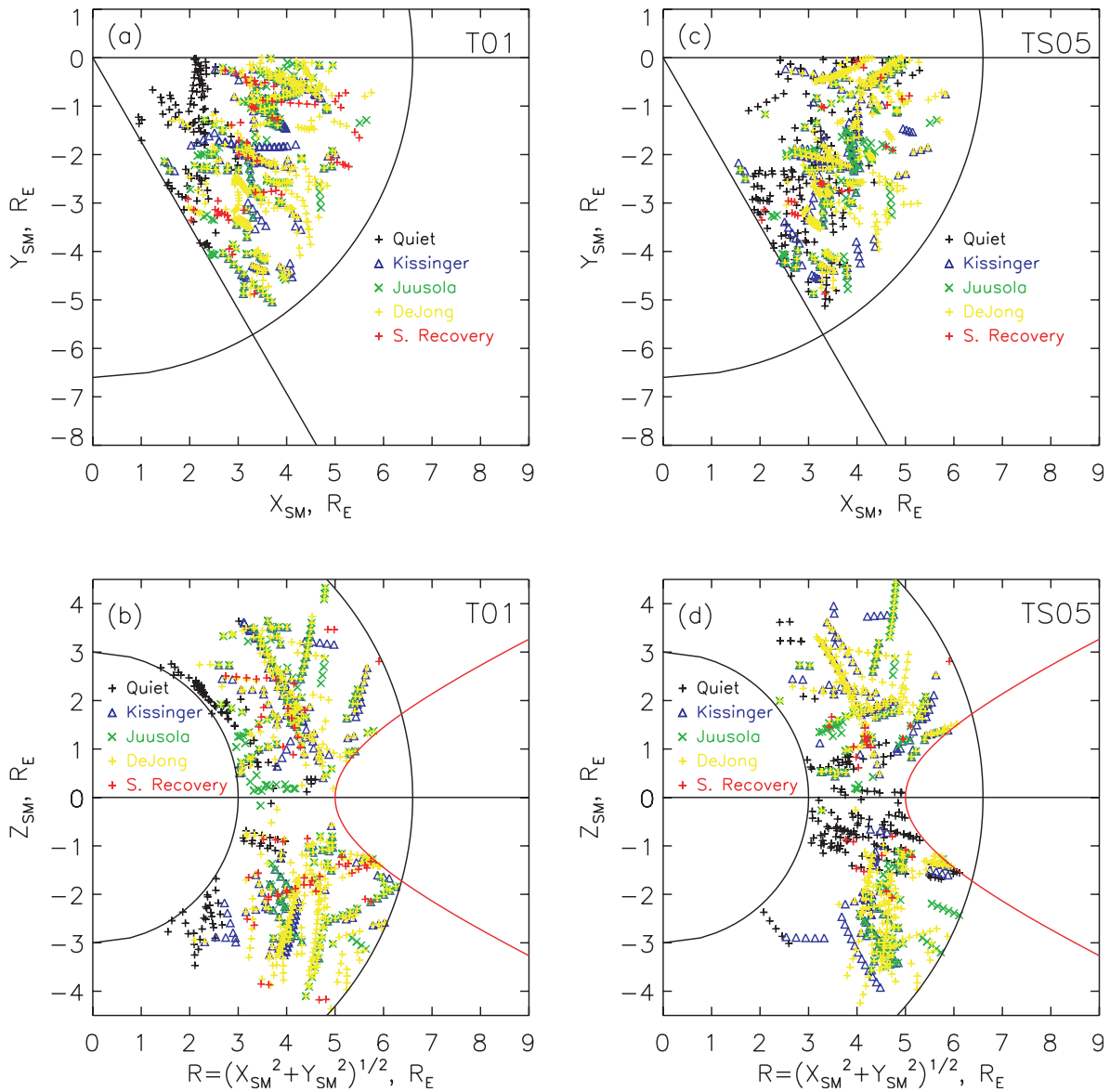


Figure 4. Spacecraft positions for different dynamic magnetosphere states when the observations were used as an input for the estimation of the SRC intensity. The curves delineate the region of the method applicability.

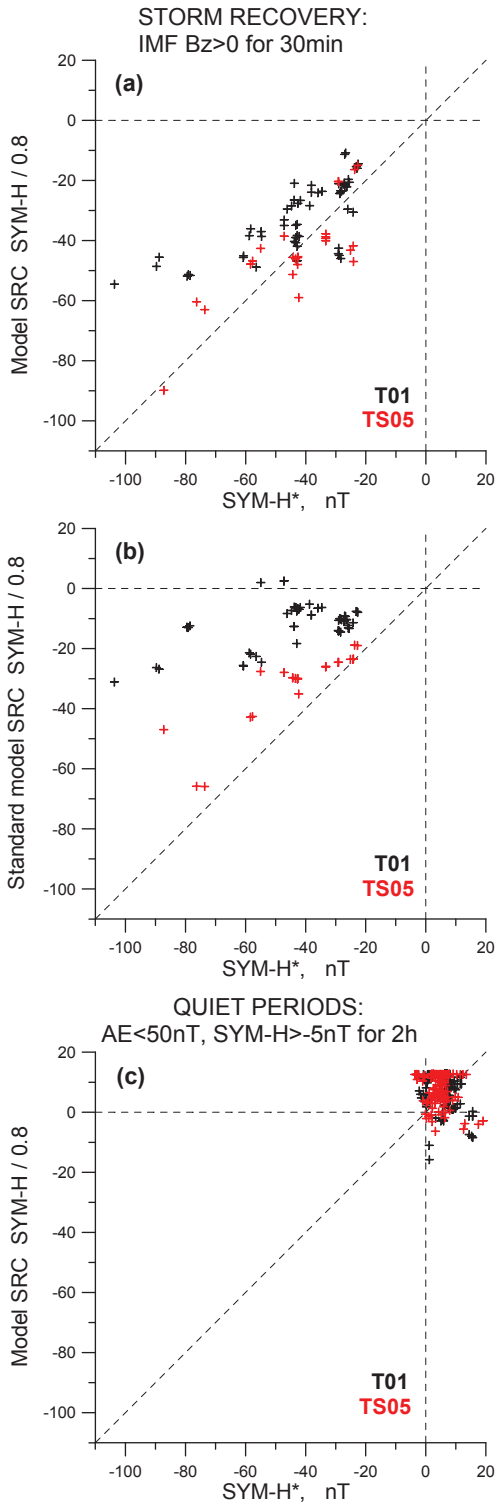


Figure 5. Contribution to SYM-H from the model SRC (with intensity determined from real observations) versus pressure corrected SYM-H index for recovery phases of geomagnetic storms (a) and quiet conditions (c). (b) Contribution to SYM-H from the standard model SRC for the same events as in (a).

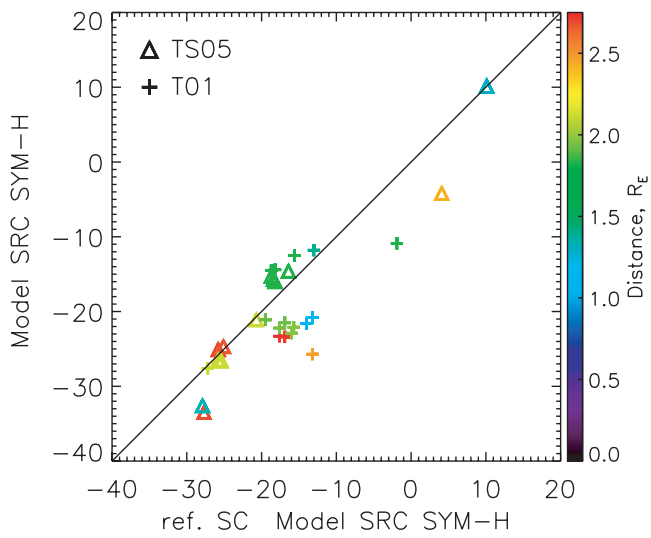


Figure 6. SRC SYM-H computed using the data of reference spacecraft versus that computed using the data of other spacecraft for the same time. Color indicates the distance between the spacecraft.

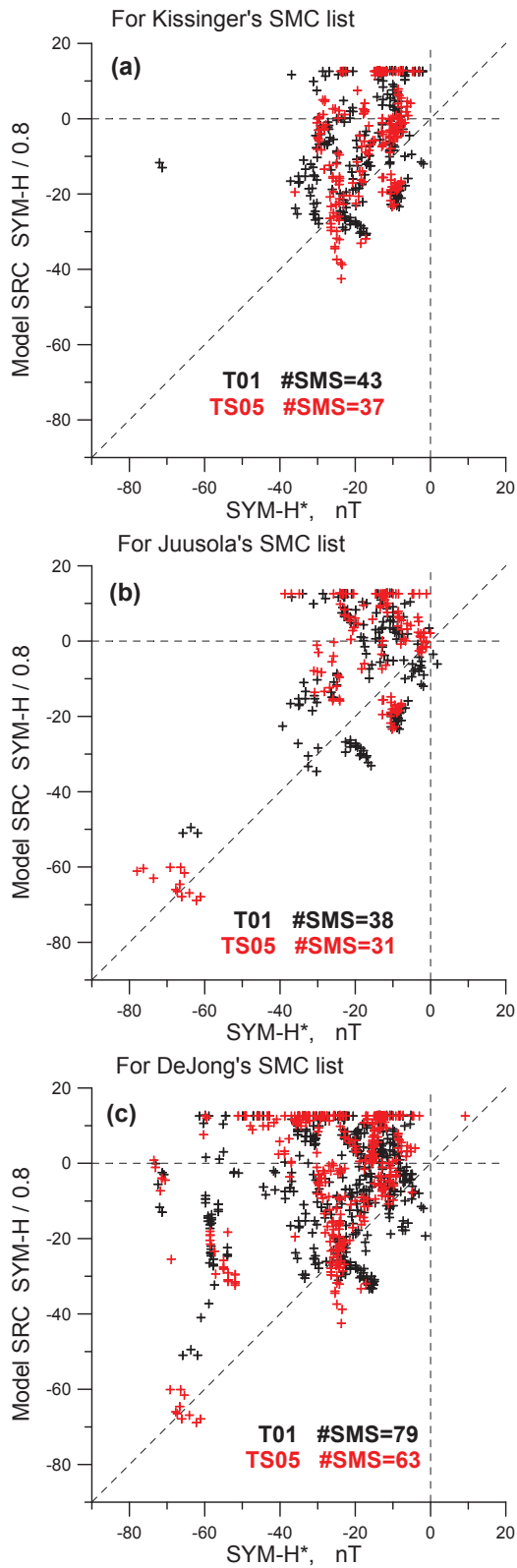


Figure 7. Model SRC contribution to SYM-H versus pressure corrected SYM-H. The legend shows the number of the individual SMC events represented in the figure.

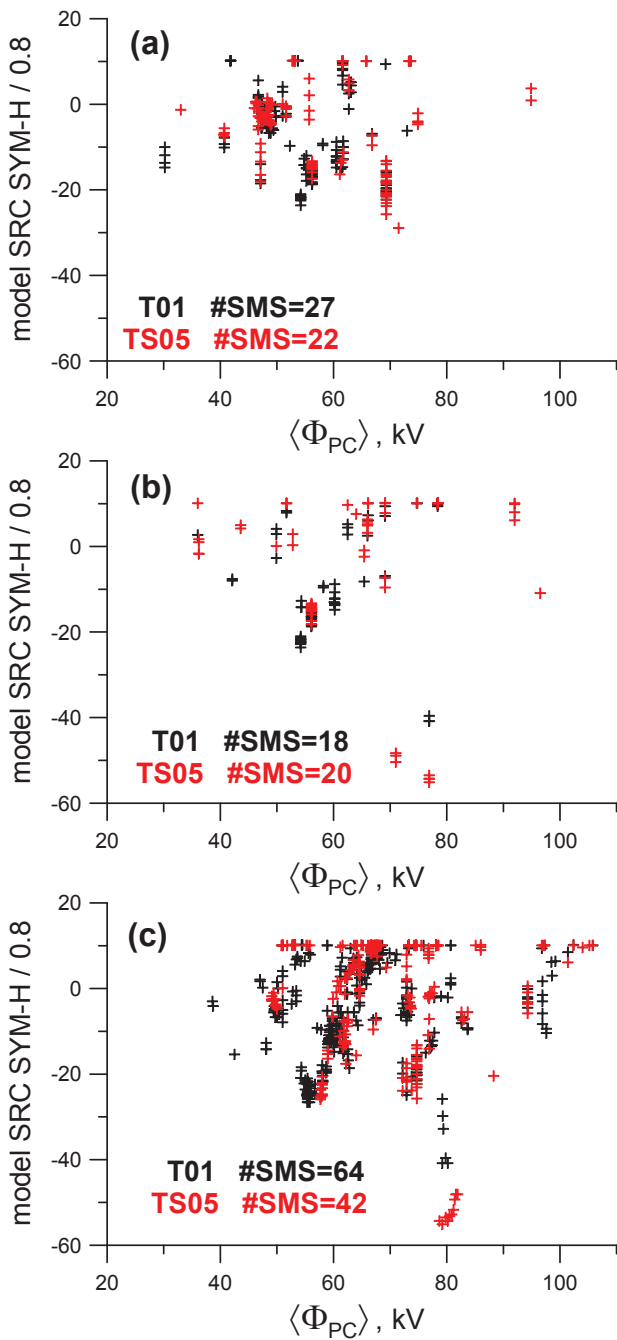


Figure 8. Model SRC contribution to SYM-H versus mean polar cap potential for the SMC events. (a) Kissinger, (b) Juusola, and (c) DeJong lists of events. The legend shows the number of the individual SMC events represented in the figure.

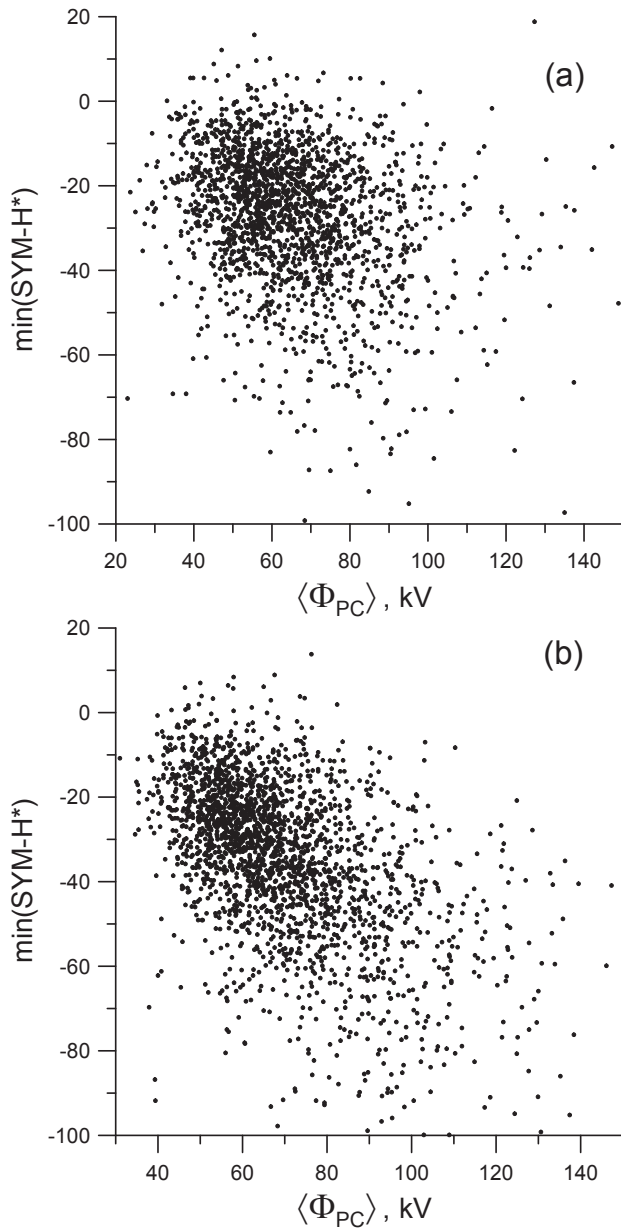
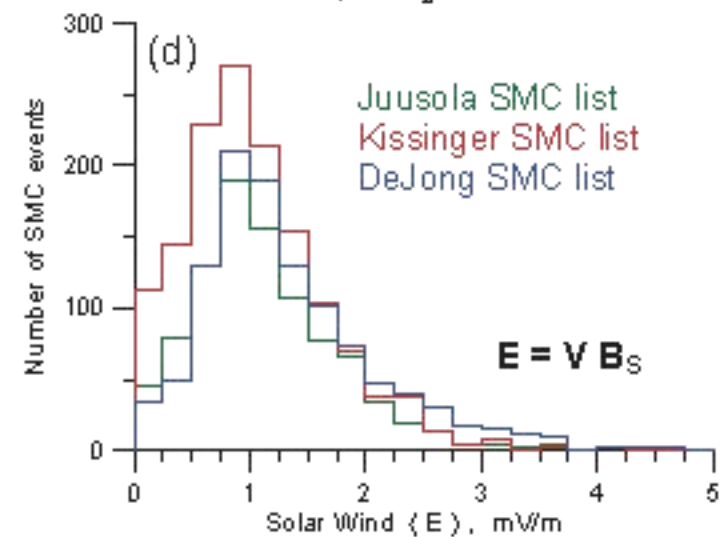
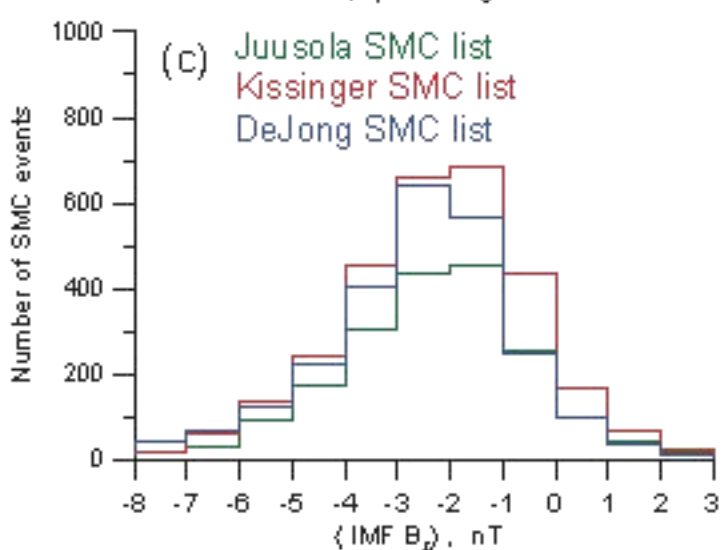
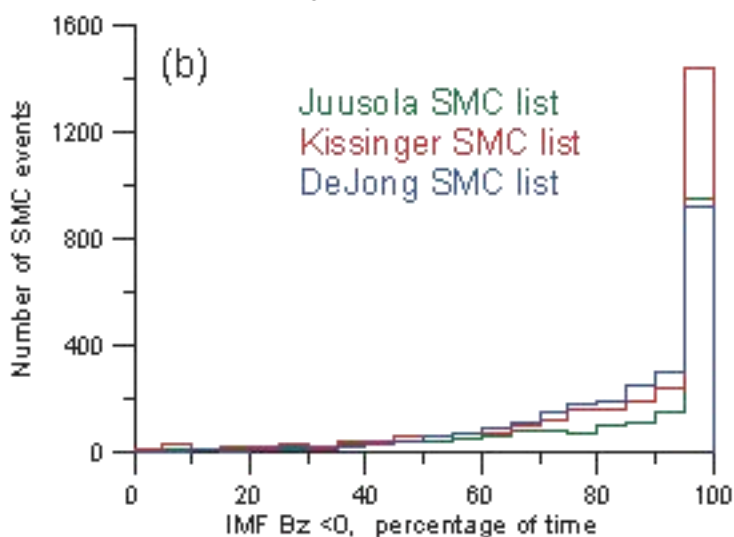
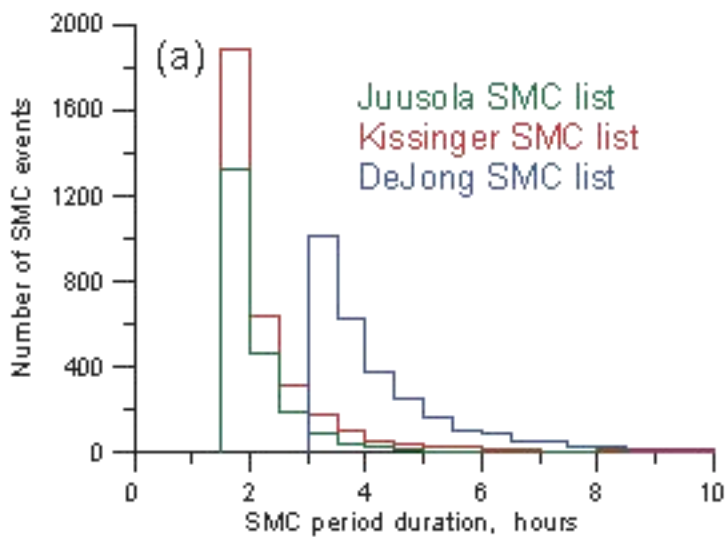
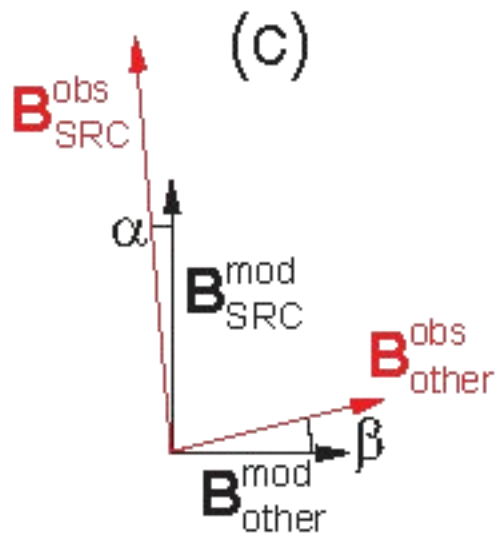
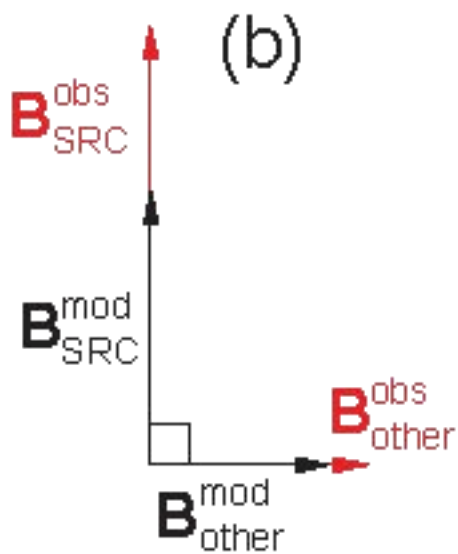
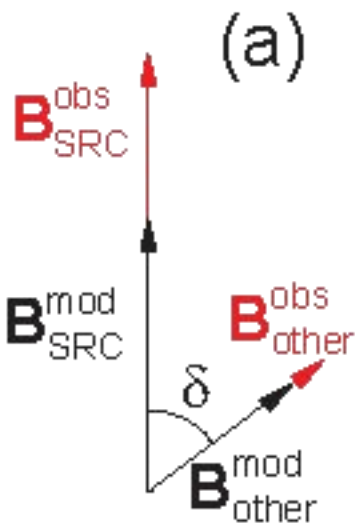
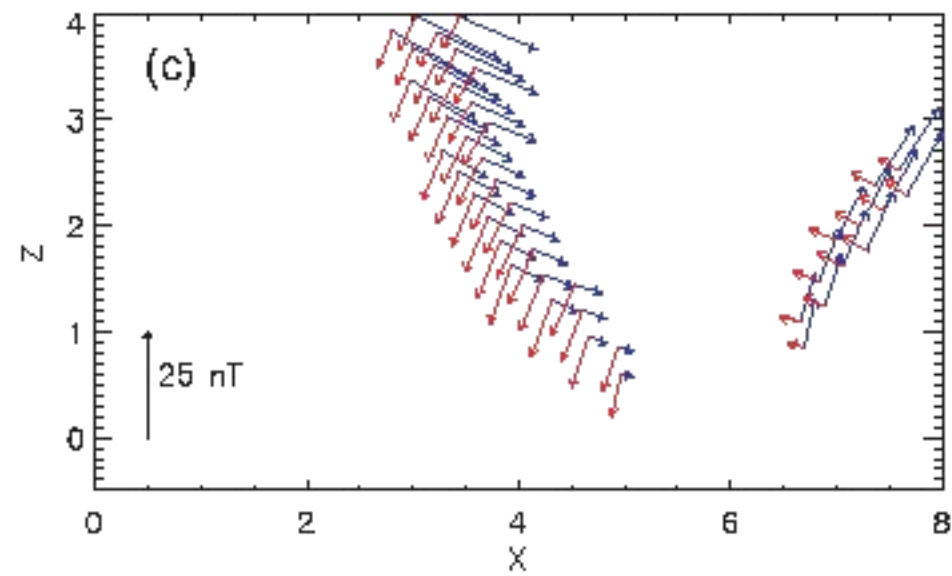
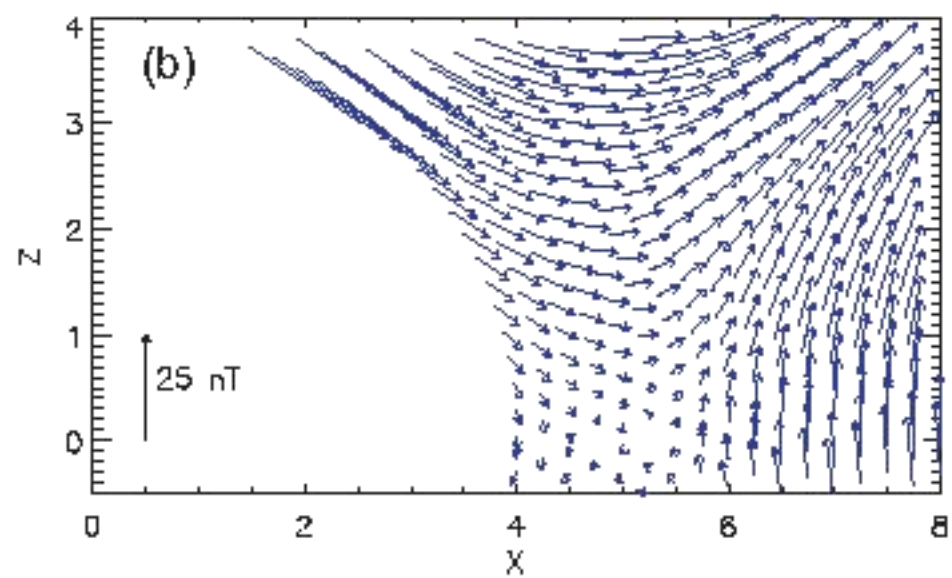
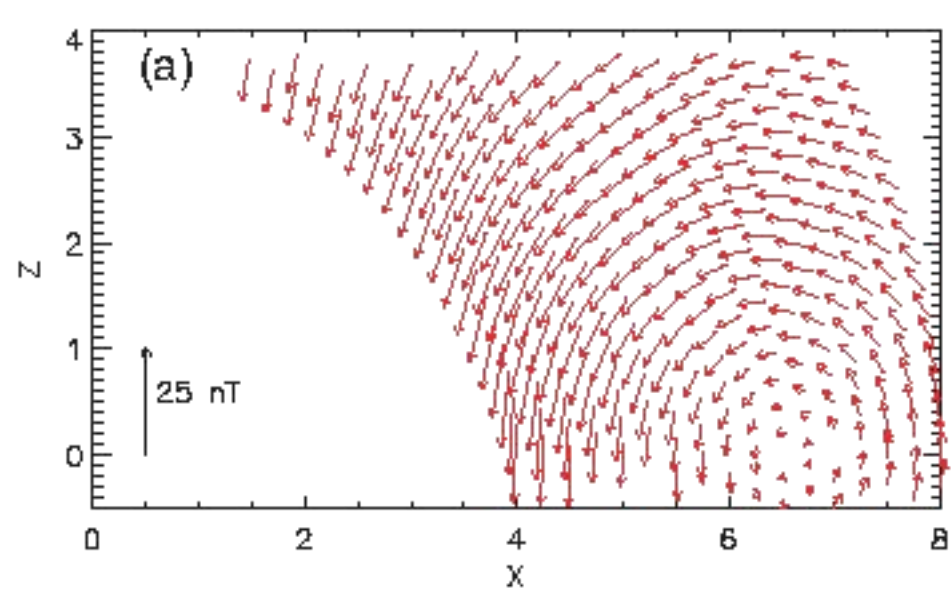
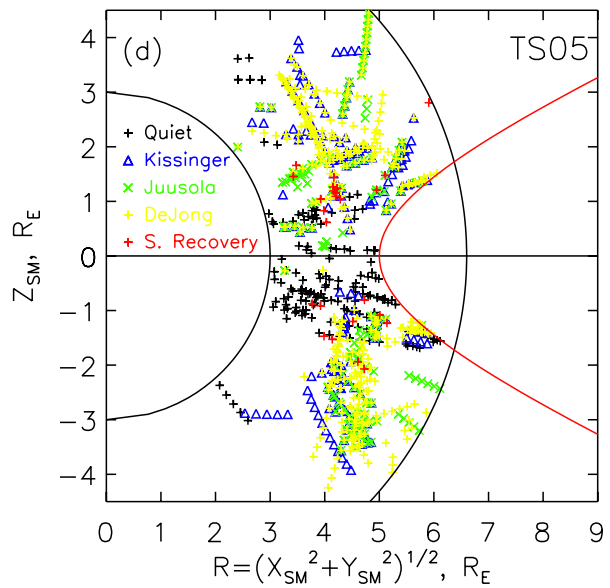
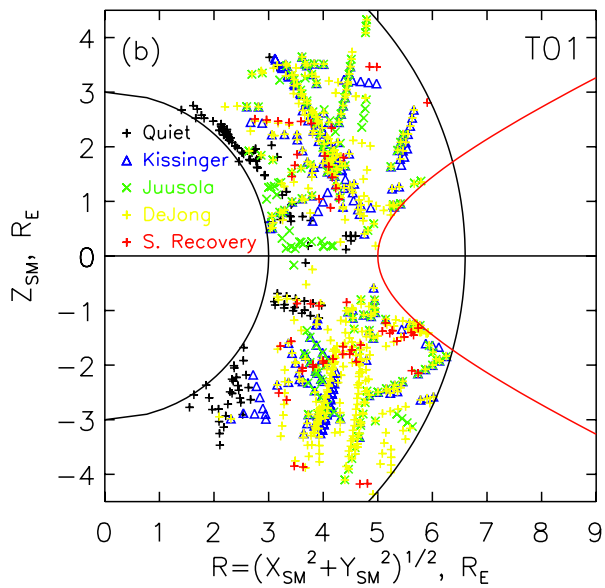
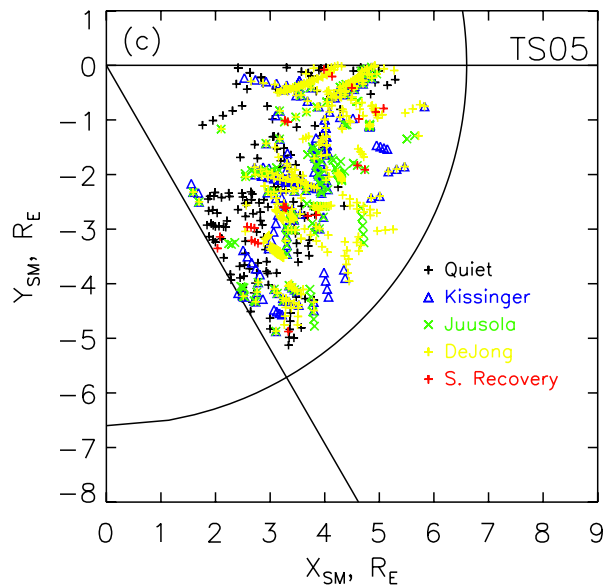
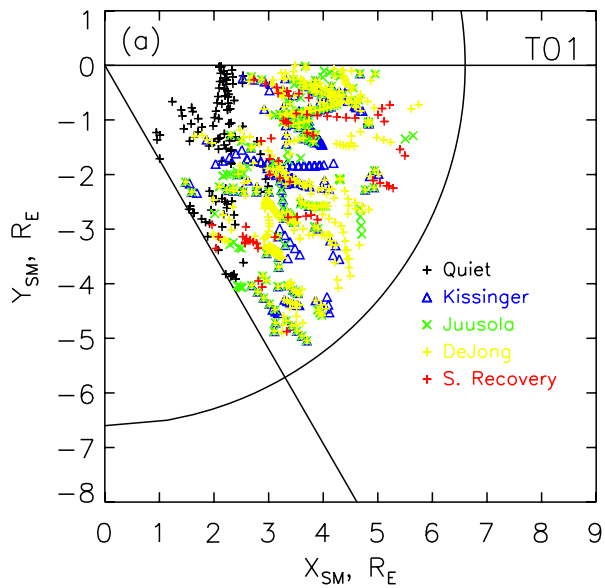


Figure 9. Minimum SYM-H* versus mean polar cap potential for the SMC events. (a) Jussola, and (b) DeJong lists of events.

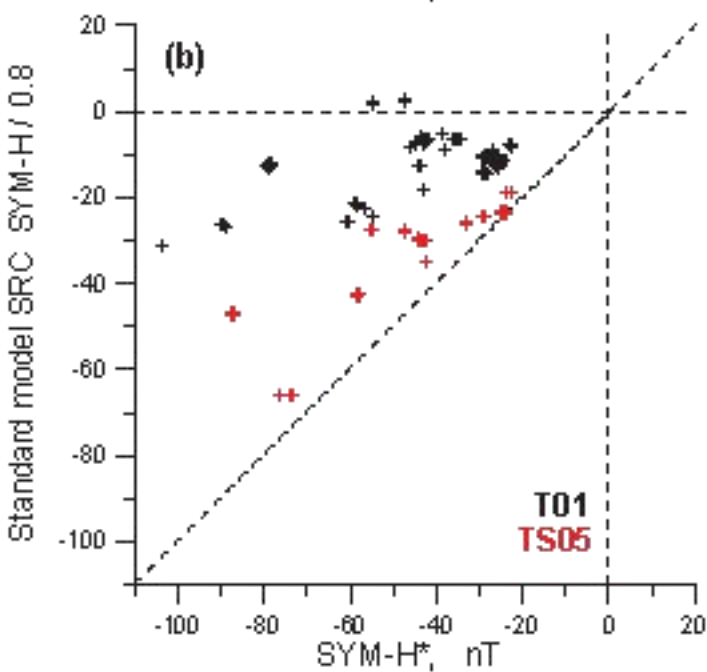
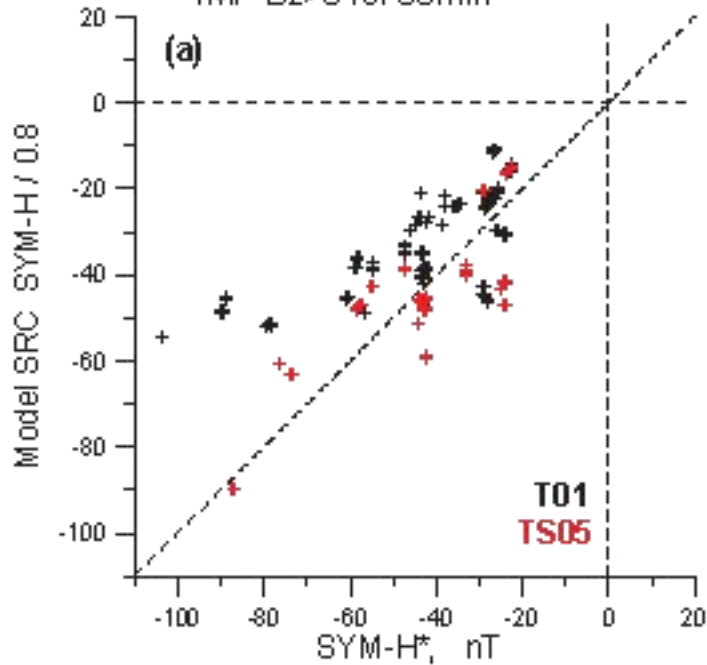




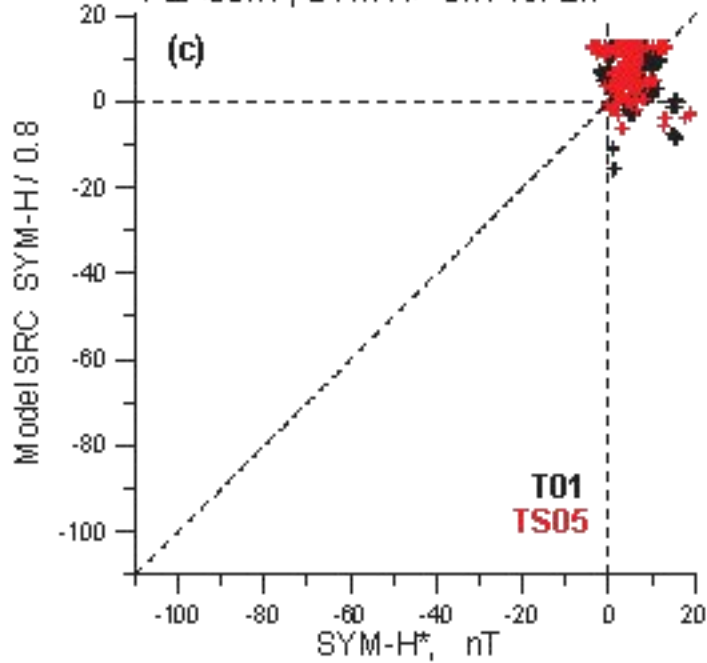


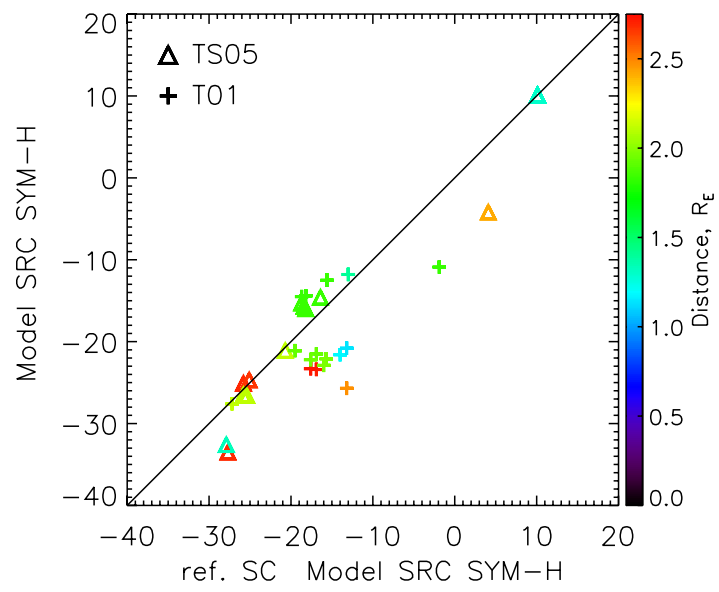


STORM RECOVERY:
IMF $B_z > 0$ for 30min

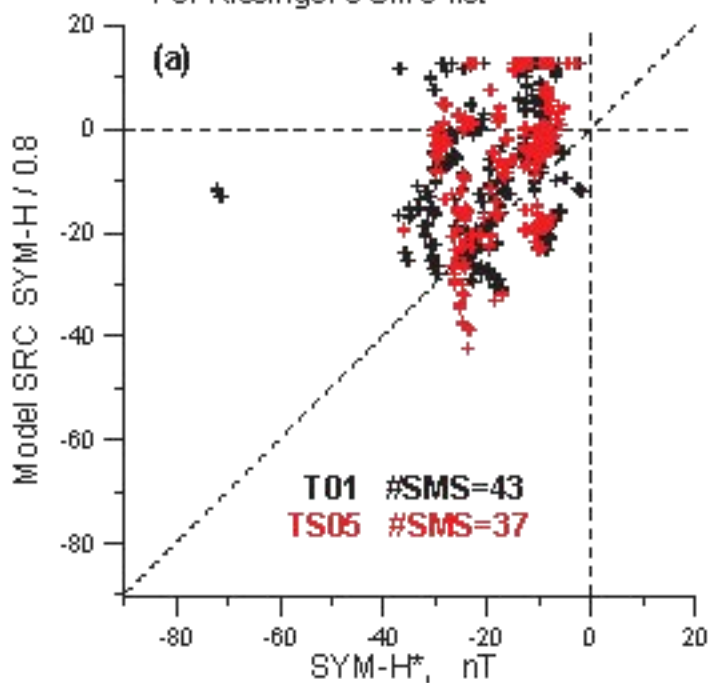


QUIET PERIODS:
 $AE < 50$ nT, $SYM-H > -5$ nT for 2h

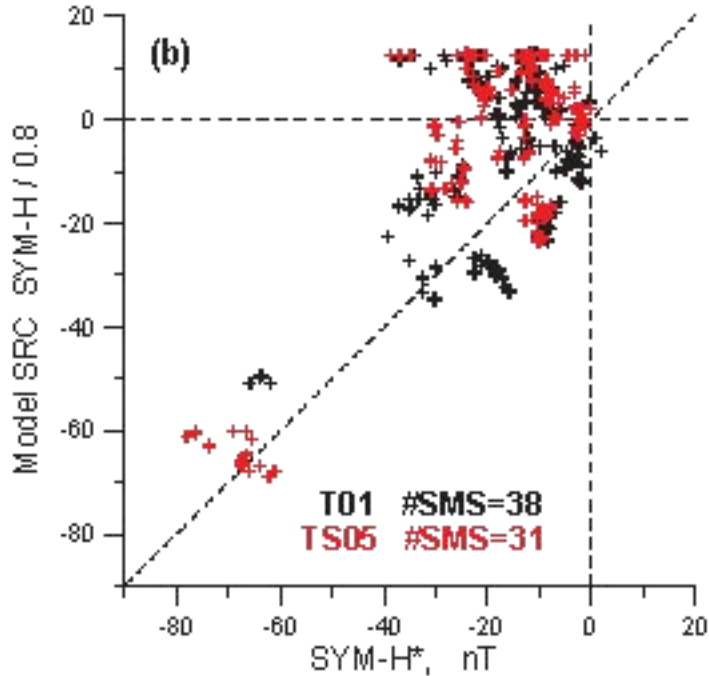




For Kissinger's SMC list



For Juusola's SMC list



For DeJong's SMC list

